STRUCTURAL STUDIES OF MATERIALS FOR HYDROGEN STORAGE

***Final report* – In-situ SR-PXD measurement: 01-02-772 Beamline BM01A**

Initial comment

The Physics Department at Institute for Energy Technology has a strong activity on hydrogen storage materials, involving many national and international collaborators. The strong position of the group is to a high degree owing to the good access to neutrons for powder neutron diffraction (PND) using the diffractometer PUS at the Institute's research reactor JEEP II.

Synchrotron power X-ray diffraction (SR-PXD) is an invaluable supplement to PND due to the superior speed and resolution. The data acquisition times are typically 3 orders of magnitude shorter using the MAR345 image plate at BM01A compared to PUS. This allows in-situ investigations of chemical reactions that we cannot possible follow with PND. The very high resolution offered at BM01B allows indexing and space group determination from complex structures where the problem with peak overlapping makes the task unmanageable with PND- or laboratory PXD data.

Thus, the predictable, long-term access to the beam lines at SNBL through the long-term projects 01-01-745 and 01-02-772, has been an invaluable supplement to our neutron diffraction facilities and the rest of our experimental activity.

Phase transformations and thermal decomposition of $Mg(BH_4)_2$ and $Ca(BH_4)_2$

$Mg(BH_4)_2$ and $Ca(BH_4)_2$ are among the most promising materials for mobile hydrogen storage with 14.9 and 11.6 w% H, respectively, and predicted favorable thermodynamics. However, their decomposition pathways have not been experimentally determined.

A sample of α-$Mg(BH_4)_2$ was heated from room temperature (RT) to 500°C with 2°C/min under dynamical vacuum in a quartz capillary fitted in a "Nordby-cell" at BM01A. Diffraction data were collected every 2 minutes on the MAR345 image plage.

Between 180 and 190 °C, most of the α-$Mg(BH_4)_2$ is transformed to β-$Mg(BH_4)_2$. However, about 20% of the sample remains as α-$Mg(BH_4)_2$ which only disappears slowly between 190 and 245°C without any further increase in the amount of β-$Mg(BH_4)_2$. Thus, this fraction of the α- $Mg(BH_4)_2$ appears to decompose without prior transformation to the β-modification.

β- $Mg(BH_4)_2$ decomposes from about 245 °C under formation of MgO, Mg and traces of MgH_2. The formation of MgO, which becomes significant above 280°C,indicates a leak in the system or reaction with the capillary. This unfortunately obscures the investigation of the pure decomposition reaction. No boron-containing phases are observed at any point.

The Bragg peaks from MgH_2 starts to increase above 360°C which is remarkable since it is well over the expected decomposition temperature. It may be explained by crystal size growth of nanosized MgH_2 which may be stabilized by encapsulation in MgO. The MgH_2 starts to decompose at 440°C.

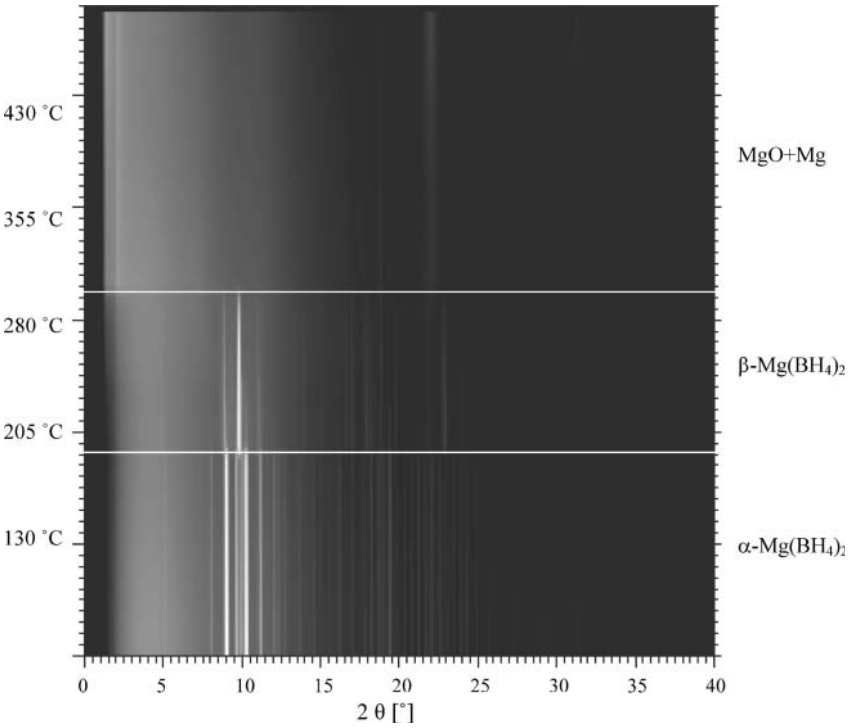

Figure 1 In-situ SR-PXD data of the thermal decomposition of $Mg(BH_4)_2$.

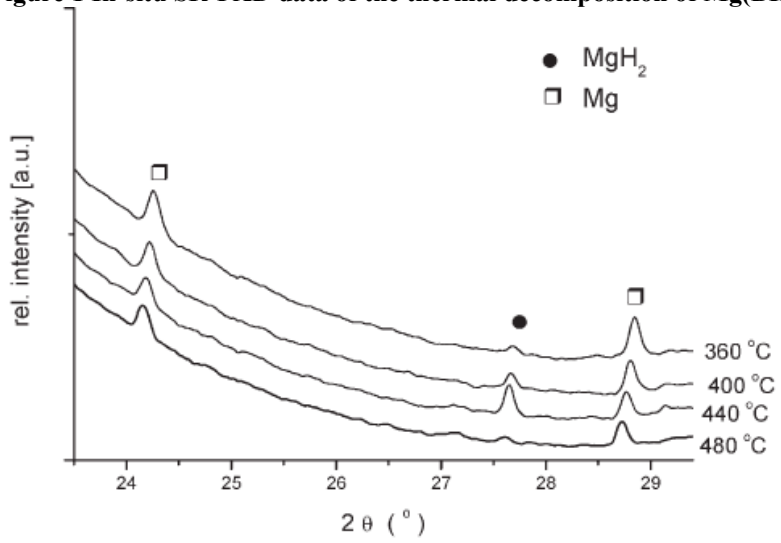

Figure 2 Formation and decomposition of MgH_2 at unusually high temperature.

A sample containing the β- and γ-modification of $Ca(BH_4)_2$ was investigated in the same way.

Parts of the γ-$Ca(BH_4)_2$ is slowly and gradually transformed to β-$Ca(BH_4)_2$ between 40˚C and 290˚C (Figure 3a). From 290˚C to 330˚C there is a faster transformation of the remaining γ-$Ca(BH_4)_2$ to a new phase. This occurs without any change in the amount of β-$Ca(BH_4)_2$ (Figure 3b) and in a temperature range where no gas desorption is detected by Temperature-Programmed Desorption (TPD). Thus, it is assumed that the phase is a new modification of $Ca(BH_4)_2$, tentatively named δ-$Ca(BH_4)_2$.

β-Ca(BH4)2 starts to decompose at 330˚C and the decomposition is completed at 380 ˚C. This correspond to the temperature range of the main gas desorption event measured by TPD. The disappearance of β-$Ca(BH_4)_2$ is accompanied by a small increase in the amount of the new "δ-$Ca(BH_4)_2$" phase, formation of a second unidentified phase, and an increased amount of CaO.

The new "δ-$Ca(BH_4)_2$" phase decomposes in the temperature range 400–480˚C. This decomposition also involves gas release according to the TPD measurement.

The final crystalline products at 500˚C are CaO (again indicating leak or reaction with capillary), CaH_2 and the unidentified phase that was formed on decomposition of "δ-$Ca(BH_4)_2$". No crystalline boron-containing phases were observed. However, EDS/SEM show that the Ca:B-ratio is unchanged in the fully desorbed sample. Thus, the boron does not disappear as diborane gas but must be present in an amorphous state.

The intermediate phase CaB_2H_2 (see ref. [1] and final report for long-term project 01-01-745) is not observed in the in-situ measurement. This is probably due to its very high reactivity towards air. The formation of CaO indicates a leak and the CaB_2H_2 may be oxidised immediately after it is formed.

The results are published in Journal of Materials Chemistry.[2]

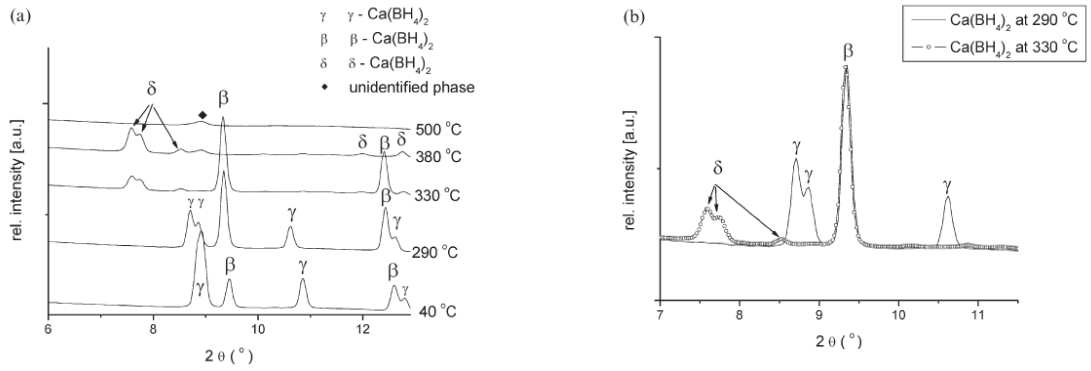

Figure 3 a) Selected integrated SR-PXD patterns during thermal decomposition of $Ca(BH_4)_2$ (see text for discussion). b) formation of "δ-$Ca(BH_4)_2$" from γ-$Ca(BH_4)_2$.

$Mg(BH_4)_2$ inflitrated in activated carbon

Nano-particles will have physical properties that differ from the bulk material when the particles size is sufficiently small. This may open up new routes to change the thermodynamics of hydrogen strorage materials.

One way to produce nano-particles is to infiltrate the material of interest into a porous medium. $Mg(BH_4)_2$ was infiltrated in activated carbon AC1 to a ratio $Mg(BH_4)_2$: AC1 of 40 : 60 (sample labeled $Mg(BH_4)_2$ / AC1).

In-situ SR-PXD patterns were collected at BM01A using the image plate detector (MAR345) with an exposure time of 30 s. The data were integrated by the Fit2D program. The sample was contained in 0.5 mm boron-silica glass capillary and heated under dynamic vacuum from 40 to 450 ^oC at a constant heating rate of 2 ^oC min^{-1}. The wavelength was λ = 0.6525 Å and the sample to detector distance d = 200 mm.

Figure 4 shows a subset of the data. We can only detect the disappearance of the α-phase at around 200 ^oC and not the structural phase transformation to the high-temperature modification β-$Mg(BH_4)_2$, observed at the temperature range of 180-190 ^oC under similar conditions in bulk. The formation of MgH_2 on decomposition is not observed either, probably due to the small particle sizes in the present system. DSC performed on this sample at the same heating rate (not shown here) confirms the phase transition from α to the high-temperature β–modification occur around 208 ^oC and as well as two decomposition steps at around 280 and 330 ^oC.

The data were collected in the April 2009 and the analysis is not yet complete.

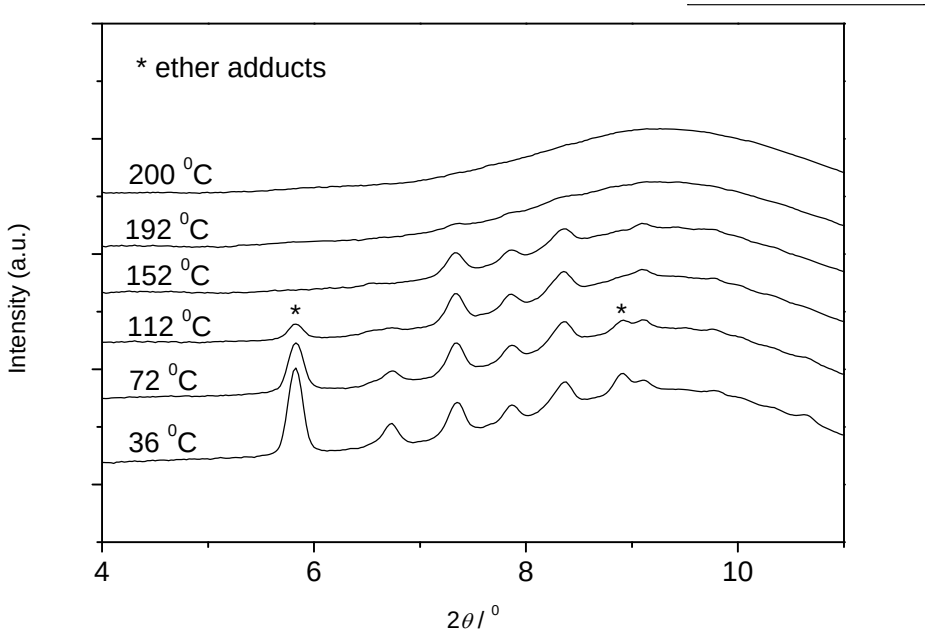

Figure 4 Selected range of the SR-PXD patterns during heating of $Mg(BH_4)_2$ / AC1 at 2 °C min^{-1}.

$LiY(BH_4)_4$ from mixture of $LiBH_4$ + YCl_3

A mixture of $LiBH_4$ and YCl_3 in the 4 : 1 ratio was ball milled for 1 h at 400 rpm in an attempt to make $LiY(BH_4)_4$. In-situ SR-PXD measured as described for $Mg(BH_4)_2$ in AC (above) confirmed the presence of two new phases at room temperature as observed by laboratory PXD. The phases are indexed and expected to be two modifications of $LiY(BH_4)_2$. The structure determination is in progress. The phases decompose around 200 °C (around scan 40, see Figure 5). Peaks of a new third phase appeared shortly at higher temperature (see scan 48 in Figure 6).

The data were collected in the April 2009 and the analysis is not yet complete.

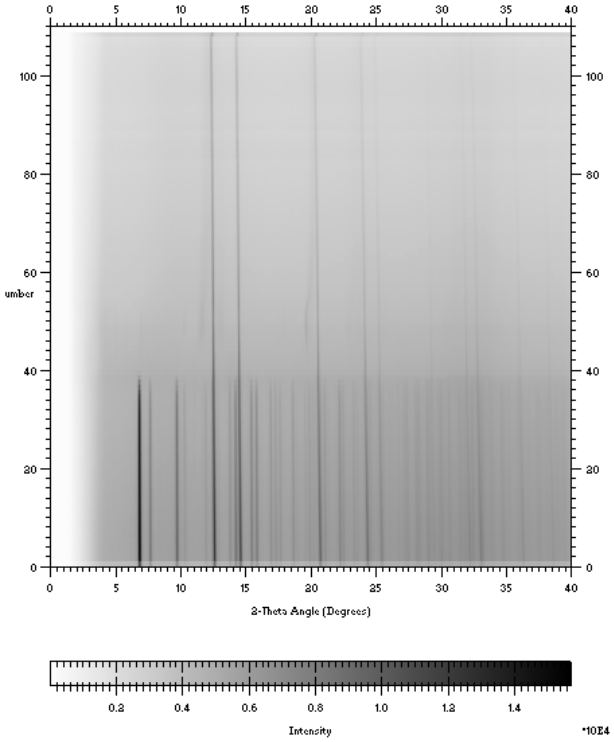

Figure 5 In-situ SR-PXD data for product after ball milling of 4 $LiBH_4$ + YCl_3

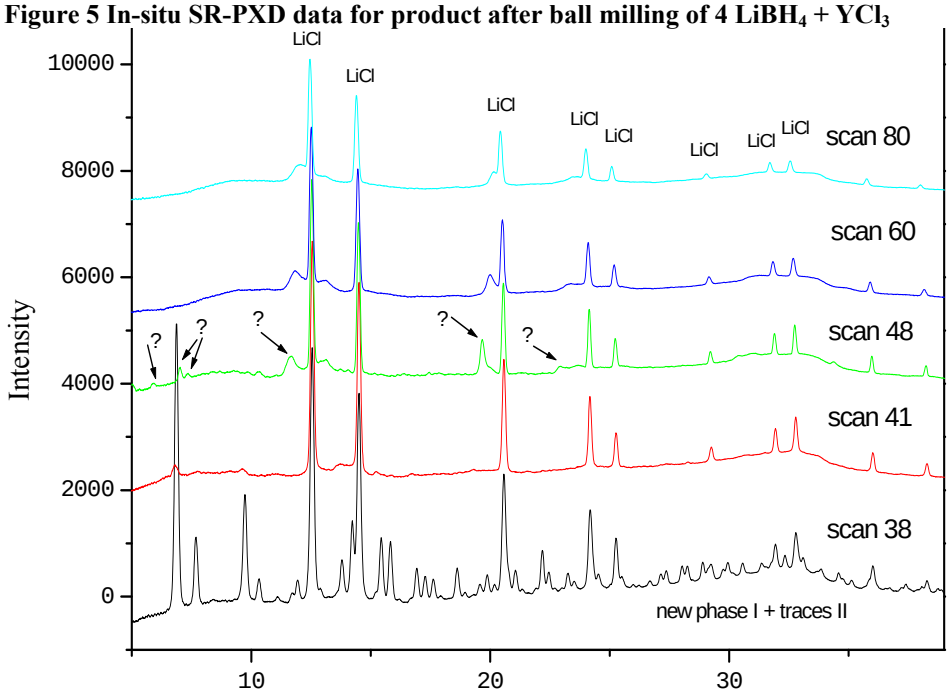

Figure 6 Selected integrated SR-PXD patterns from Figure 5. Peaks marked by '?' are from an unidentified decomposition product.

Phase transformations and thermal decomposition of alane

Alane, AlH_3, is interesting for hydrogen storage due to the very high hydrogen capacity (10.1 w%H) which is released at a moderate temperature (~120˚C).

Six structure modifications of AlH_3 are reported, but only four of them, α-, α'- β- and γ-AlD_3, have been synthesised reproducibly. The crystal structures of α'- β- and γ-AlD3 were determined from PND and high-resolution SR-PXD data from an earlier long term project at BM01B. It has been debated in the literature which modification is the most stable. Experimental studies indicate that α-AlD_3 is the most stable modification but DFT calculations indicate that β- is more stable than α-AlD_3.

In the present investigation, the phase transformation and thermal decomposition of the modifications α-, α'- β- and γ-AlD_3 are investigated by in-situ SR-PXD at BM01B. Heating rates of 1˚C/min were used. Quantitative phase analysis was performed for every recorded diffraction pattern see the phase evolution.

The phase evolution on heating for a sample containing a mixture of α- and α'-AlD_3 is shown in Figure 7. Decomposition of the α'-phase starts around 80 ˚C as seen from a decrease its relative phase proportion and onset of Al formation. The α-phase starts to decompose around 95˚C. The α' and α are fully decomposed at 140 and 160 ˚C, respectively. There is no indication of phase transformation from α-AlD_3 to α'-AlD_3 or visa verca.

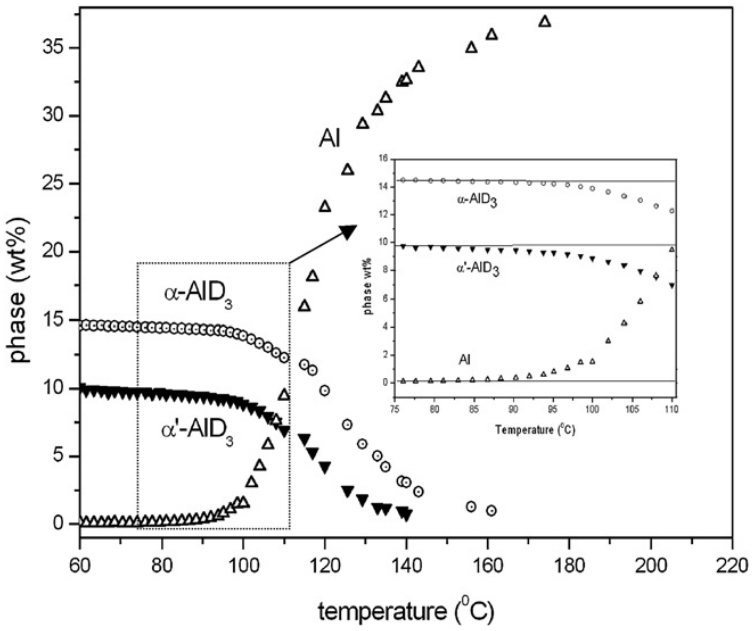

Figure 7 Phase evolution on heating for a sample containing α- and α'-AlD_3 as found from in-situ SR-PXD and quantitative phase analysis.

The thermal decomposition of γ-AlD_3 proceeds differently. Figure 8 shows the phase evolution for a sample of 90% γ- and 10% α-AlD_3. From about there is clearly a transformation from γ- to α-AlD_3 as the amount of the former decrease while the latter increase correspondingly. From about 105˚C, the rate of reduction of the γ-AlD_3 decrease, but it increases again from 115˚C (see inset Figure 8) which coincide with the onset of Al formation. Thus, γ-AlD_3 decomposes directly to Al and D_2 from this temperature. All γ-AlD_3 has disappeared at 120˚C where the α-AlD_3 starts to decompose. The decomposition is

complete at 150 ˚C. The reason for the different in the temperature range for decomposition of α-AlD_3 in the two measurements, are not clear.

The phase evolution of β-AlD_3 (90% purity, 10% γ-AlD_3) is shown in Figure 9. The β-phase shows a complete transformation to α-AlD_3 and no direct decomposition is observed. The α-phase decomposes in a similar way as in the γ+α-sample. Interestingly, the γ-AlD_3 impurity shows a similar features as for the γ-AlD_3 sample above, with an inital rapid conversion to α-AlD_3 which slows down before a direct decomposition to Al and D_2 starts. Thus, this peculiar behaviour seems to be an characteristic feature for γ-AlD_3.

From these investigations, it is clear that α-AlD_3 is the most stable modification among α-, α'-β- and γ-AlD_3.

The results are published in two papers in Journal of Physical Chemistry C[3] and Journal of Materials Science.[4]

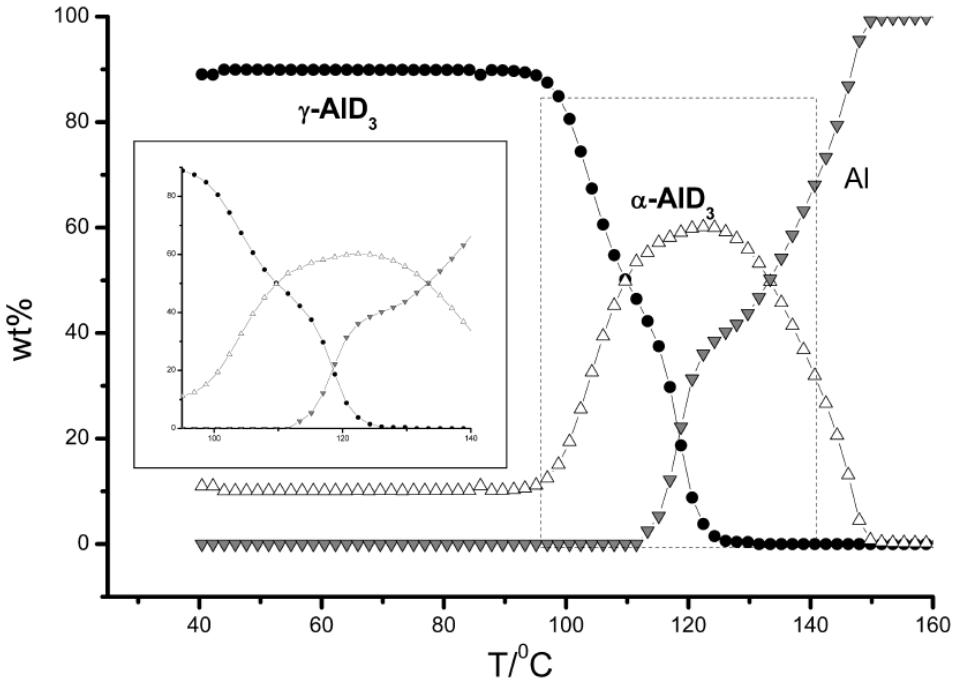

Figure 8 Phase evolution on heating a sample of 90% γ-AlD_3 and 10% α-AlD_3 as found from in-situ SR-PXD and quantitative phase analysis.

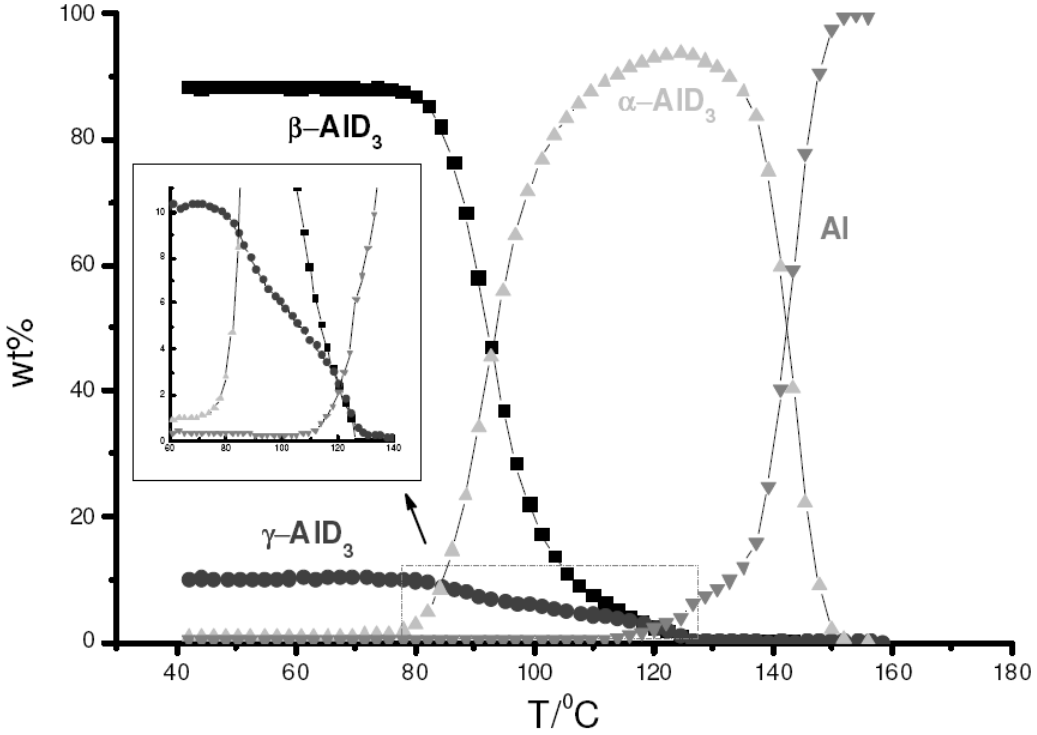

Figure 9 Phase evolution on heating a sample of 90% β-AlD_3 and 10% γ-AlD_3 as found from in-situ SR-PXD and quantitative phase analysis.

Anion substitution with fluorides in AlD_3

In this study fluorides were added to the synthesis of alane to investigate a possible substitution by the formation of a mixed solid solution phase like $AlD_{3(1-x)}F_x$. Such anion substitution could change the stability and thermodynamics of alane.

Alane can be made by cryomilling a mixture of $3LiAlD_4 + AlCl_3 \rightarrow 4AlD_3 + 3LiCl$. Two samples were made, where AlF_3 or NaF, respectively, were added to the starting materials to yield a molar molar F:D ratio of 1:1. The samples were cryomilled for 1 h in a Spex Freezer mill. In-situ SR-PXD data was collected at SNBL station A.

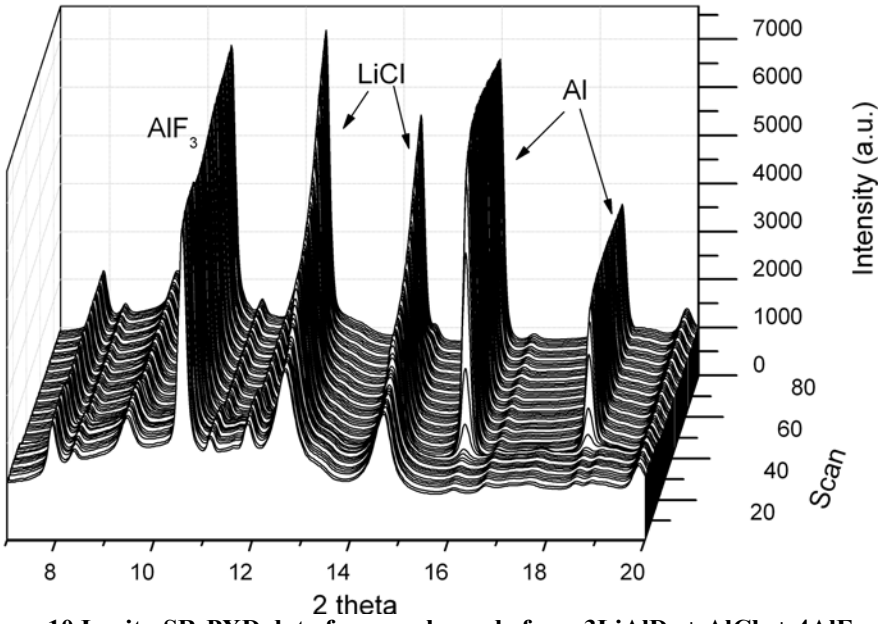

Figure 10 In-situ SR-PXD data for sample made from $3LiAlD_4 + AlCl_3 + 4AlF_3$

The sample made from $3LiAlD_4 + AlCl_3 + 4AlF_3$ was heated from RT to 360°C at a rate of 2°C/min. The data are not fully analyzed, but preliminary investigations show that AlD_3 has not been formed in the synthesis. The sample contains mainly LiCl and AlF_3. The amount of AlF_3 is nearly constant in the whole measurement, while the content of LiCl increases significantly. At 130-140°C a large amount of Al is formed. These results clearly show that there are other phases present, probably with overlapping peaks. Some peaks indicate the presence of $LiAlCl_4$, $LiAlF_4$ or Li_3AlF_6. Further data analyses are needed to clarify the phase decomposition in the sample.

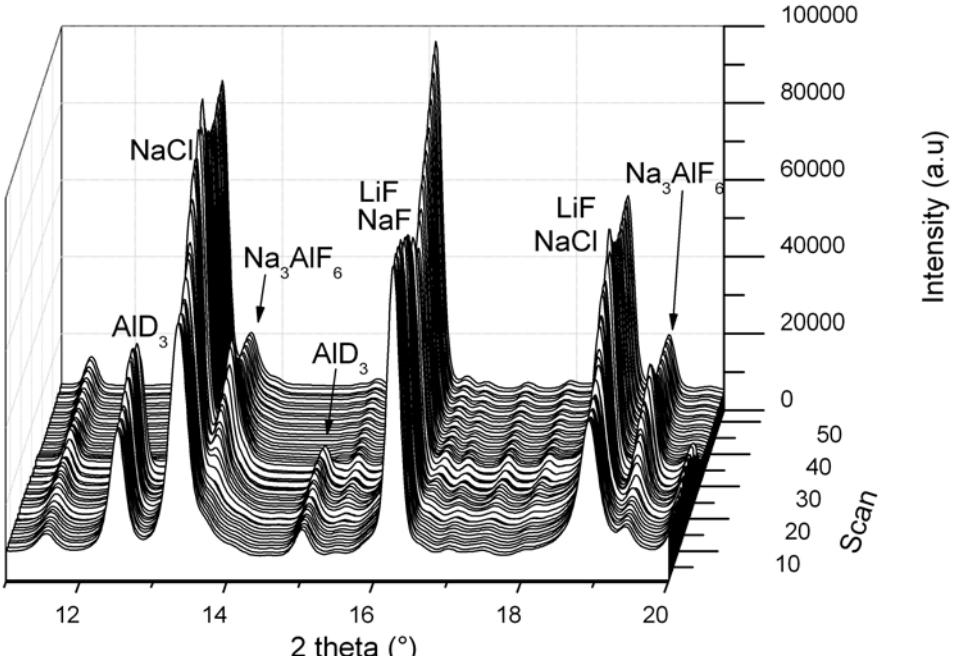

Figure 11 In-situ SR-PXD data for sample made from 3LiAlD4 + AlCl3 + 12NaF

The sample made from $3LiAlD_4 + AlCl_3 + 12NaF$ was heated from RT to 230°C at a rate of 2°C/min. The data are not fully analyzed, but preliminary investigations show that several phases are present at the start of the experiment; AlD_3, NaCl, NaF and LiF. The decomposition of AlD_3 occurs in the range 120-140°C, as expected. The content of NaCl is increasing, while NaF is decreasing, and formation of Na_3AlF_6 is detected.

The data were collected in the April 2009 and the analysis is not yet complete.Detailed Rietveld analysis is required to investigate whether anion substitution occurs in the alane-phase.

Thermal decomposition of Na_2LiAlH_6

The thermal decomposition of the pure and TiF_3-doped Na_2LiAlH_6 was investigated by in-situ SR-PXD at BM01A.

Pure Na_2LiAlH_6 and Na_2LiAlH_6 doped with 2mol% TiF_3 decompose in a similar manner to LiH, NaH and Al from around 200 to 250°C. Samples with 10mol% TiF_3 behave quite differently. Firstly, a significant proportion (20mol%) of the Na_2LiAlH_6 is decomposed when the TiF_3 is added, yielding Na_3AlH_6 and Al. Moreover, the parts of remaining Na_2LiAlH_6 decompose to Na_3AlH_6 and Al before the final decomposition to NaH, LiH and Al. This is particularly pronounced in a sample that has been dehydrogenated and rehydrogenated (cycled).

A manuscript for publication of the results are in the final stage of preparation and will be submitted to Journal of Alloys and Compounds.

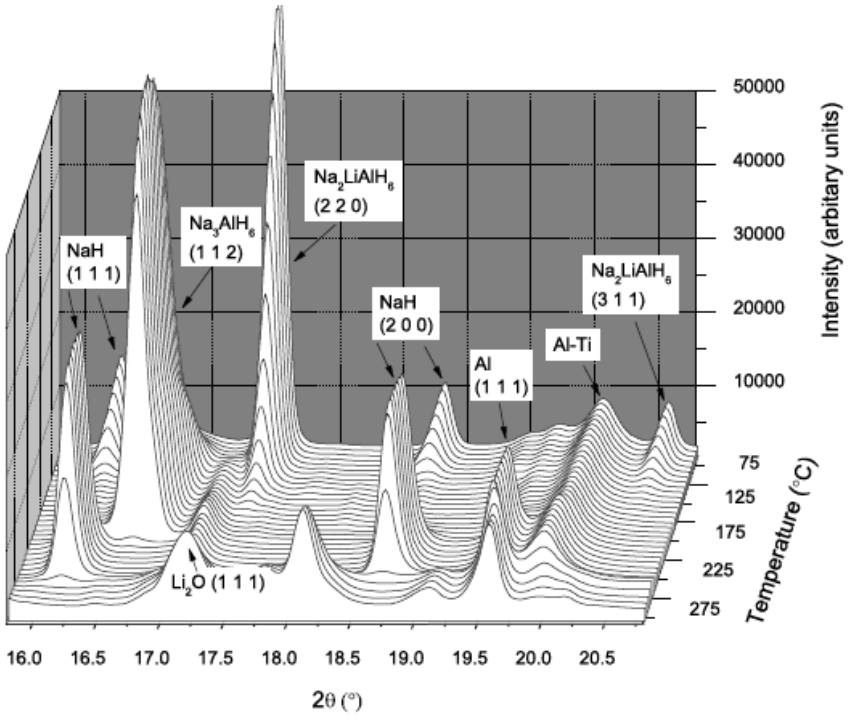

Figure 12 In-situ SR-PXD data for thermal decomposition of cycled Na_2LiAlH_6 + 10 mol% TiF_3. Note the substantial increase in the Na_3AlH_6 amount prior to decomposition.

Thermal decomposition of $NaAl(NH_2)_4$

Amides, NH_2^- - containing salts, have been considered for hydrogen storage since the discovery of reversible hydrogen uptake in Li_3N under formation of $LiNH_2$ and LiH.

The amide $NaAl(NH_2)_4$ was prepared by direct reaction of $NaAlH_4$ and NH_3 under ball milling. SR-PXD at BM01A at ambient temperature showed a sample of high purity, as shown in the Rietveld fit in Figure 13 (the structure model was taken from literature).

The in-situ SR-PXD (Figure 14) was performed simultaneously with Raman spectroscopy (Figure 15). There are no changes in the SR-PXD patterns, besides peak shift due to thermal expansion, until 110°C which correspond to the first desorption event where approximately ½ NH_3 pr. formula unit is desorbed (measured separately with thermogravimetry (TG) and mass spectroscopy(MS)). This leads to a complete amorphisation of the sample, as seen by the absence of Bragg peaks. However, the Raman signal barely change as a result of the amorphisation which means that the amorphous decomposition product also contain amide ions.

According to the TG/MS measurements, there is a steady loss of NH_3 (reflected by a gradual decrease in the NH_2 Raman signal) from the first desorption event up to 230°C where a new peak in the NH_3 desorption is observed. This desorption event is reflected in both the SR-PXD and the Raman data. The diffuse scattering measured by SR-PXD change its characteristics, indicating formation of a different amorphous substance. At the same time, the Raman signal corresponding to NH_2-bending and stretching is lost. The TG/MS indicate that 2 NH_3 pr. formula unit are lost at this point. The amorphous phase above 230°C is thus probably Na-Al imide, $NaAl(NH)_2$.

A manuscript for publication of the results is in the final stage of preparation.

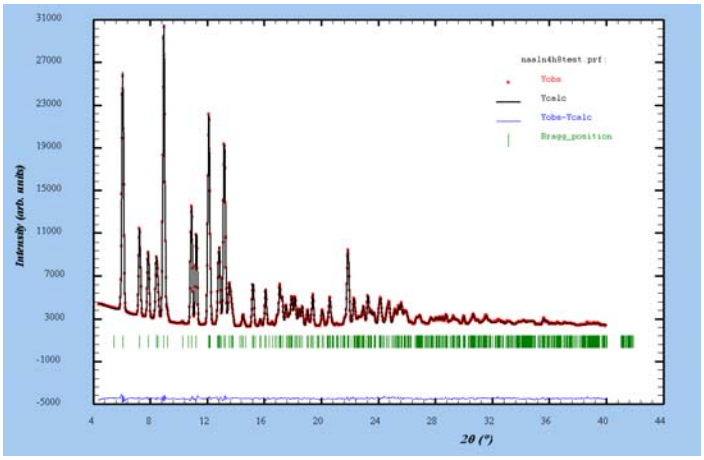

Figure 13 Rietveld fit of SR-PXD data (RT) showing a $NaAl(NH_2)_4$ sample of high purity.

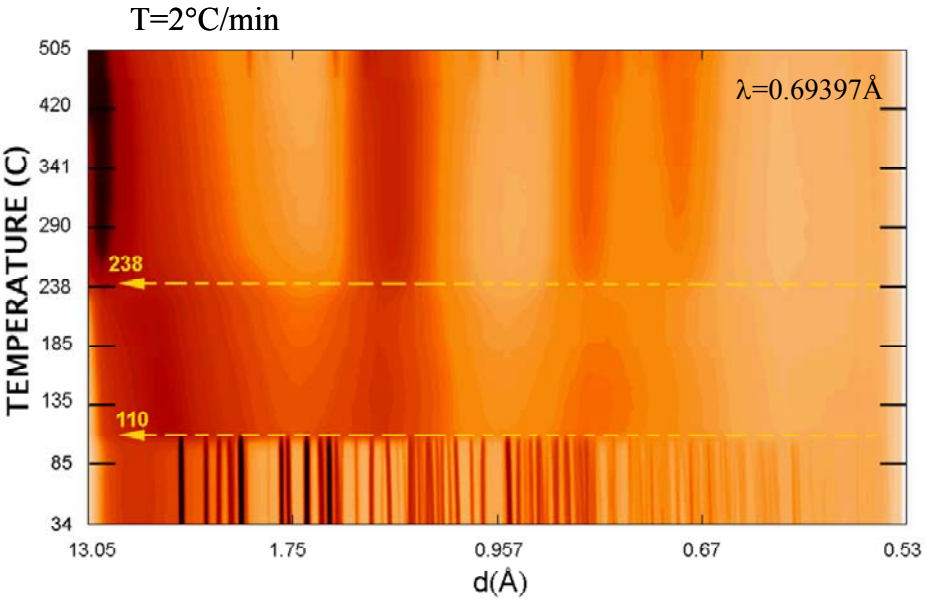

Figure 14 In-situ SR-PXD data for thermal decomposition of $NaAl(NH_2)_4$.

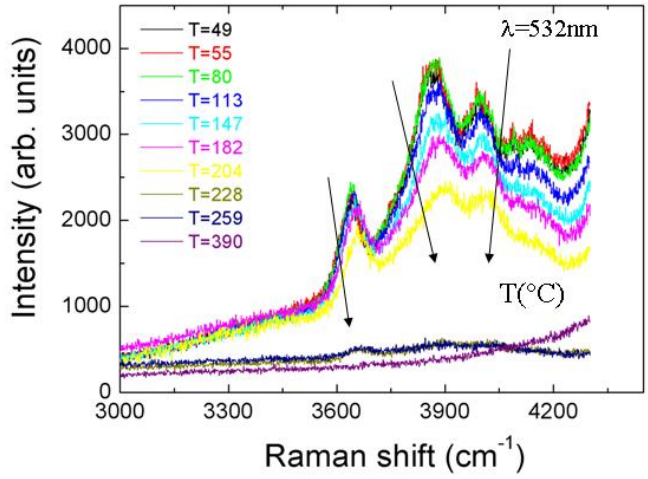

Figure 15 In-situ Raman data for thermal decomposition of $NaAl(NH_2)_4$. The signals above 228 °C are associated to bending and stretching modes of NH_2.

$^7Li_{1+x}MgN_2D_{3-x}$

The solid solution of $^7Li_{1+x}MgN_2D_{3-x}$ with x=0, 1, 1.66 and 2 was produced by mixing ^7LiD and $Mg(ND_2)_4$ in 3:3, 6:3, 8:3 and 9:3 molar ratio, respectively. The mixture was then ball milled and heat treated at 200 ^{0}C. Mass spectrometry measurements have shown that increasing the LiD/MgN_2D_2 ratio suppresses release of ammonia and promote release of hydrogen. Furthermore, increasing the content of LiD lowers the hydrogen desorption temperature (Figure 16).

The determination of structural change will give the opportunity to understand and possibly design new light complex metal hydride for hydrogen storage. We have studied the structure of the solid solution $Li_{(1+x)}MgN_2D_{3-x}$ with x equal respectively to 0, 1, 1.66 and 2 by the mean of PND and SR-PXD (BM01B, long term project 01-01-745) at room temperature, by using deuterium and lithium-7 isotope to reduce incoherent neutron scattering and neutron absorption, respectively..

In-situ synchrotron X-ray powder diffraction was performed at BM1A. Simultaneously Raman spectra were collected and focused on the imides stretching mode.

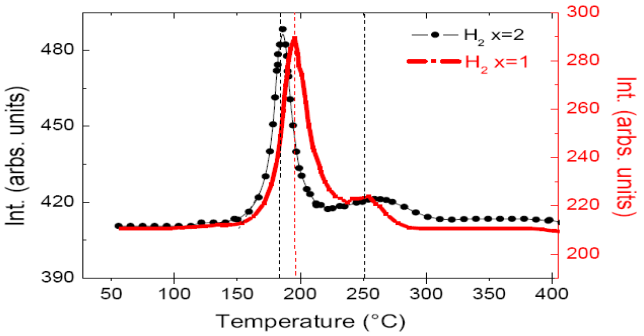

Figure 16 Evolution of the Mass spectrometer signal assigned to the H_2 release of $Li_{(1+x)}MgN_2D_{3-x}$ with x=1 and 2 versus temperature (respectively in red and black curves).

Rietveld refinement of the PND pattern over the whole composition range reveals that the structure can be described by a solid solution which is isomorphic as the $Li_{1.2}Mg_{0.8}N$. Li/D occupancies changes respectively with x content. High disorder on the D sites is to found.

Preliminary analysis of the diffraction patterns of the thermal decomposition, over the whole composition range indicates that there is two distinct mechanism involved in the desorption one for x<1 and the other one for x>1. For x<1, the diffraction pattern is dominated by amorphous material. For x>1 Characteristic temperature evolution of the diffraction pattern are shown in fig. 3. They present typical 3 zones (I, II and III in Figure 18).

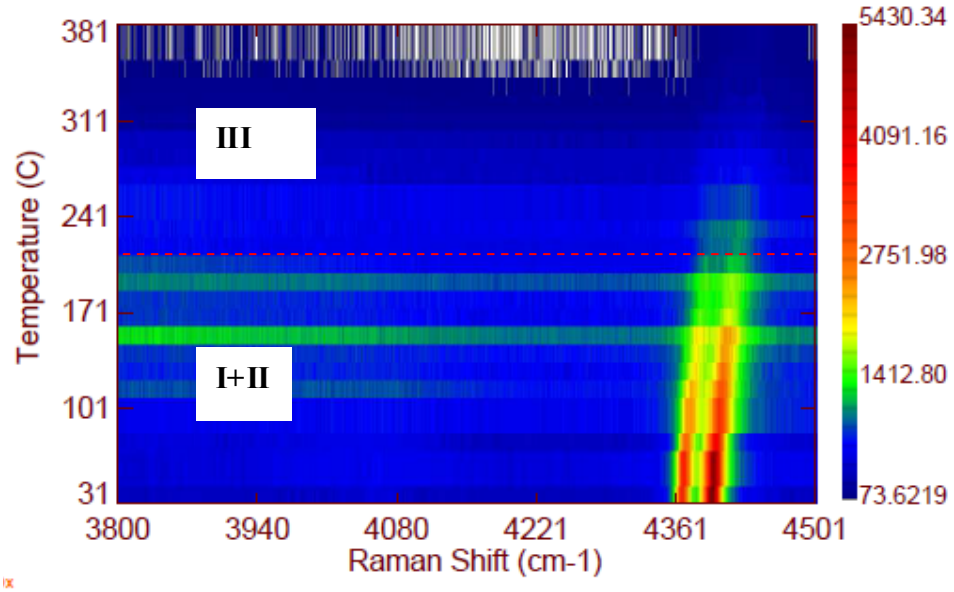

Figure 17 Color plot representing the evolution of Raman spectra of Li_3MgN_2D versus temperature (x-axis represent the raman shift, the y-axis the temperature).

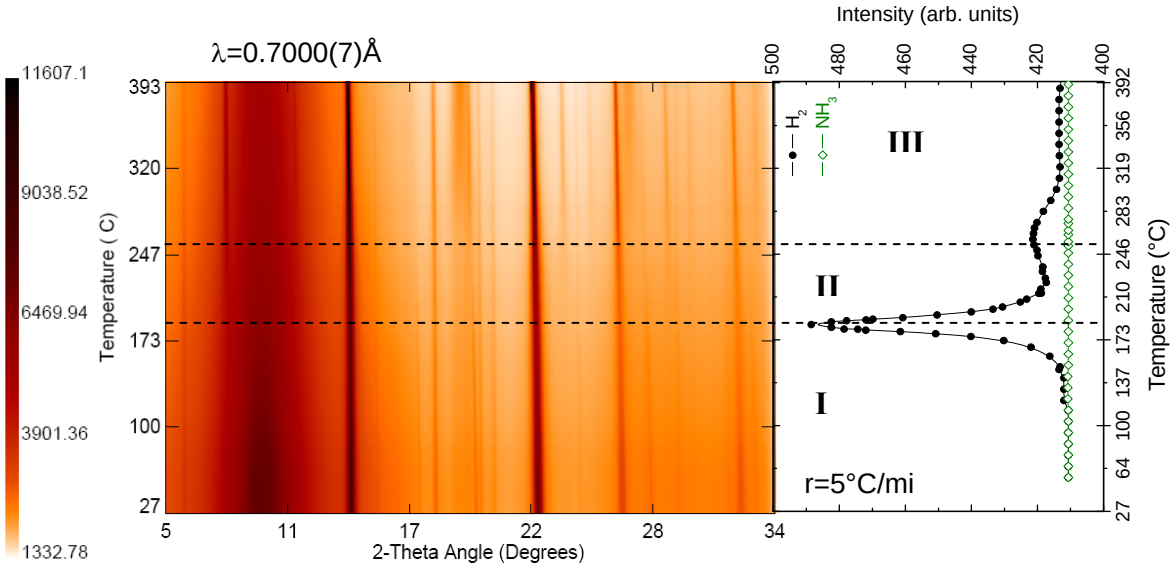

Figure 18 Color plot representing the evolution of $Li_3MgN_2D_1$ diffraction pattern versus temperature (left panel) (x-axis represent the 2θ(degree), the y-axis the temperature and the color the intensity in the left scale). The right panel is the TPD coupled with mass spectrometry analysis of the desorbed gas. The black and green curves in the right figure monitor the temperature evolution of mass spectrum meter signal of H_2 and NH_3 respectively.

The temperature evolution of the Raman spectra for all the composition sample show a similar trend as presented in Figure 17. Only Raman stretching bands for imides are observed up to the around the 230^{0}C (Zone I and II) suggesting that above this temperature no more imides is present.

For x>1, the initial compound starts to release NH_3 at around 120 ^{0}C and transform continuously into its isotructural nitride counterpart $Li_{1.2}Mg_{0.8}N$ as illustrated by the decrease in intensity of the Raman spectra (Figure 17). Above 170 ^{0}C, Mg_3N_2 is observed and phase coexistence is observed between 170 and 250 ^{0}C. In this temperature range 3 main phases are coexisting: $Li_{1.2}Mg_{0.8}N$, Mg_3N_2 and $Li_{(1+x)}MgN_2D_{3-x}$. Due to the low hydrogen scattering cross section and identical cell parameter between the LiMg nitride and deuteride, no phase quantity analysis was possible. In the zone III, crystallisation and formation pure Mg is observed.

A manuscript for publication is under preparation.

Thermal decomposition of $Mg_2(Fe_{0.5}Co_{0.5})D_{5.5}$

The synthesis and structural characterization of the quaternary deuteride $Mg(Fe_{0.5}Co_{0.5})D_{5.5}$ is described in the report for long-term project 01-01-745.

The thermal decomposition of the phase was investigated by in-situ SR-PXD at BM01B. The raw data are shown in Figure 19. Bragg peaks from Mg, which indicate the onset of decomposition, start to appear around 500K (230°C). Around 600 K (330^{o}C) the peaks from the quaternary deuteride start to disappear quickly and they have completely disappeared at 610 K. The decomposition products are Mg and FeCo solid solution.

The result is published in Nanotechnology [5].

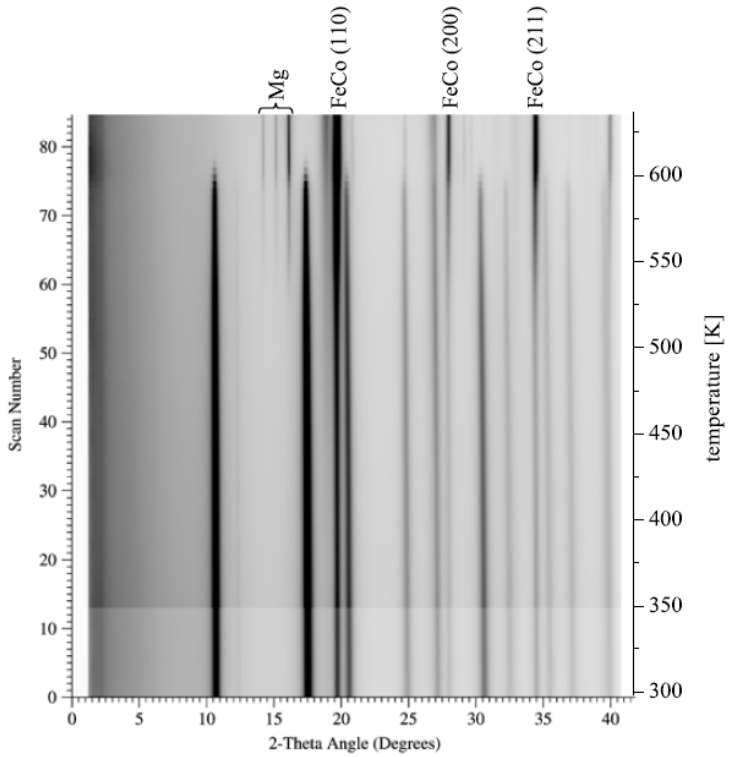

Figure 19 In-situ SR-PXD data for thermal decomposition of $Mg_2(Fe_{0.5}Co_{0.5})D_{5.5}$

References to publications from long-term project 01-02-772

[1] Riktor, M.D.; Sørby, M.H.; Chłopek, K.; Fichtner, M.; Hauback , B.C.: The identification of an hitherto unknown intermediate phase CaB_2H_x from decomposition of $Ca(BH_4)_2$. Journal of Materials Chemistry **DOI: 10.1039/B818127F** (2009)

[2] Riktor, M.D.; Sørby, M.H.; Chlopek, K.; Fichtner, M.; Buchter, F.; Zuettel, A.; Hauback, B.C.: In situ synchrotron diffraction studies of phase transitions and thermal decomposition of Mg(BH4)(2) and Ca(BH4)(2). Journal of Materials Chemistry **17** (2007) 4939-4942

[3] Grove, H.; Sørby, M.H.; Brinks, H.W.; Hauback, B.C.: In situ synchrotron powder X-ray diffraction studies of the thermal decomposition of beta- and gamma-AlD3. Journal of Physical Chemistry C **111** (2007) 16693-16699

[4] Sartori, S.; Opalka, S.M.; Lovvik, O.M.; Guzik, M.N.; Tang, X.; Hauback, B.C.: Experimental studies of alpha-AID(3) and alpha '-AID(3) versus first-principles modelling of the alane isomorphs. Journal of Materials Chemistry **18** (2008) 2361-2370

[5] Deledda, S.; Hauback , B.C.: Formation mechanism and structural characterization of the mixed transition-metal complex hydride $Mg_2(FeH_6)_{0.5}(CoH_5)_{0.5}$ obtained by reactive milling. Nanotechnology **20** (2009) 204010

Additional publications where measurements from long-term project 01-02-772 plays a minor role

a) Riktor, M.D.; Deledda, S.; Herrich, M.; Gutfleisch, O.; Fjellvåg, H.; Hauback , B.C.: Hydride formation in ball-milled and cryomilled Mg–Fe powder mixtures. Materials Science and Engineering B **158**(2009) 19-25